Risks, Wissenschaftliche Auswertungen, Berlin, Germany, 2001, pp. 400–408.
3. Houghton, J. T. *et al.* (eds), IPCC, *Climate Change 2001. The Scientific Basis*, Cambridge University Press, Cambridge, UK, 2001, p. 881.
4. Hansen, J. L. *et al.*, Earth's energy imbalance: confirmation and implications. *Science*, 2005, **308**, 1431–1435.
5. IPCC, *Climate Change 2007: The Physical Science Basis*, Summary for Policymakers, 2007, p. 21.
6. Kulkarni, A. V., Randhawa, S. S. and Sood, R. K., A stream flow simulation model in snow covered areas to estimate hydro-power potential: a case study of Malana nala, H.P., Proceedings of the First International Conference on Renewable Energy – Small Hydro, Hyderabad, 1997, pp. 761–770.
7. Kulkarni A. V., Randhawa, S. S. and Sood, R. K., A stream-flow simulation model in snow-covered areas to estimate hydro-power potential, Proceedings of International Conference on Hydro Power Development, 1998, pp. 70–82.
8. Kulkarni, A. V., Randhawa, S. S., Rathore, B. P., Bahuguna, I. M. and Sood, R. K., Snow and glacier melt runoff model to estimate hydropower potential. *J. Indian Soc. Remote Sensing*, 2002, **30**, 221–228.
9. Kulkarni, A. V. and Rathore, B. P., Snow cover monitoring in Baspa basin using IRS WiFS data. *Mausam*, 2003, **54**, 335–340.
10. Kulkarni, A. V., Singh, S. K., Mathur, P. and Mishra, V. D., Algorithm to monitor snow cover using AWiFS data of RESOURCESAT-1 for the Himalayan region. *Int. J. Remote Sensing*, 2006, **27**, 2449–2457.
11. Upadhyay, D. S., Sharma, J. K., Ray, B., Purohit, M. K. and Rajput, R. K., A conceptual model for glacier melt. Proceedings of National Meeting on Himalayan Glaciology, New Delhi, 5–6 June 1989, pp. 45–56.
12. Kulkarni, A. V., Rathore, B. P., Mahajan, S. and Mathur, P., Alarming retreat of Parbati glacier, Beas basin, Himachal Pradesh. *Curr. Sci.*, 2005, **88**, 1844–1850.
13. Kulkarni, A. V., Mass balance of Himalayan glaciers using AAR and ELA method. *J. Glaciol.*, 1992, **38**, 101–104.
14. Chaohai, L. and Sharma, C. K., Report on 1st expedition to glaciers in the Pumqu (Arun) and Poiqm (Bhote–Sun Kosi) river basins, Xizang (Tibet), China, Science Press, Beizing, China, 1988, p. 192.
15. Nye, J. F., The response of glaciers and ice-sheets to seasonal and climatic changes. *Proc. R. Soc. London, Ser. A*, 1960, **256**, 559–584.
16. Johannesson, T., Raymond, C. F. and Waddington, E. D., Timescale for adjustment of glaciers to changes in mass balance. *J. Glaciol.*, 1989, **35**, 355–369.
17. Martinee, J. and Rango, A., Parameter values for snowmelt runoff modelling. *J. Hydrol.*, 1986, **84**, 197–219.
18. Bilello, M. A., Regional and seasonal variations in snow cover density in the USSR, CRREL Report 84–22, Cold Regions Research and Engineering Laboratory, Hanover, New Hampshire, USA, 1984.

ACKNOWLEDGEMENTS. We thank Dr Ajay, Group Director, MESG/SAC and Dr T. J. Majumdar, Head, ESHD/MESG/SAC, Ahmedabad for their support and suggestions. We also thank Prof. M. N. Patel, Principal LDCE/Gujarat University, Ahmedabad for his suggestions.

Received 16 October 2008; revised accepted 1 September 2009

A high-Si, high-Ca spinel-like phase from mantle peridotite: a report from Cretaceous ophiolite of Rutland Island, Andaman–Java subduction complex

Tapan Pal[1], Biswajit Ghosh[2,*] and Anindya Bhattacharya[2]

[1]Petrology Division, Eastern Region, Geological Survey of India, Kolkata 700 091, India
[2]Project: Andaman and Nicobar, Opp. WSA, ER, Geological Survey of India, Kolkata 700 091, India

We report here exsolved phase with unusual composition (SiO_2: 14–22 wt%, CaO: 4–10 wt% and Cr_2O_3: 17–21 wt%) from mantle peridotite of the Cretaceous ophiolite of Rutland Island in the Andamans. This high-Si, high-Ca bearing spinel-like phase occurs in two modes as fine blebs (<1–3 μ) within exsolved blebs of diopside and fine lamellae (<1–7 μ) within the orthopyroxene host along with lamellae of diopside and Cr-spinel. The BSE image exhibiting a tonal character as well as the chemistry intermediate of Cr-spinel and diopside suggests that this phase exsolved from pigeonite at an intermediate stage before the exsolution of fine lamellae of Cr-spinel and diopside in the orthopyroxene host.

Keywords: Andaman, Mantle peridotite, Rutland Island, spinel-like phase.

SiO_2 can enter spinel structure by replacing Al_2O_3. Experiments demonstrate that a maximum of 28 wt% SiO_2 could be present as solid solution in Al–Si spinel structure[1]. SiO_2 solubility in spinel of lherzolite to harzburgite composition with olivine–orthopyroxene–spinel-clinopyroxene assemblage can increase in certain physico-chemical conditions. We report here a high-Si, high-Ca spinel-like new phase (*n*-spinel) from mantle peridotites represented by lherzolite to diopsidic harzburgite of the supra subduction zone ophiolite sequence of Rutland Island in the Andamans. An assemblage of exsolved grains of clinopyroxene–Cr-spinel–*n*-spinel occurs within large orthopyroxene porphyroclast of the mantle peridotites. The *n*-spinel also occurs within thick blebs of exsolved clinopyroxene. Apart from those exsolved phases, symplectites of pyroxene and spinel are also present in the mantle peridotites. The exsolved grains are formed during cooling process but symplectites of pyroxene and spinel are usually explained as the product of garnet breakdown due to decompression during the uprise of mantle[2–4]. The present observation of an intermediate phase in pyroxene–spinel stability field could address many problems related to the stability of spinel and Ca–Si solubility in spinel structure. This study has a signifi-

*For correspondence. (e-mail: bghosh_geol@hotmail.com)

cant impact in the spinel–pyroxene stability field in geological, material sciences and industrial use. Petrography, SEM and EPMA studies have been undertaken to characterize the unusual spinel-like new phase and host rock petrogenesis.

The Rutland Island is situated to the south of the South Andaman Islands, in the Bay of Bengal. The chain of Andaman and Nicobar group of islands represents the central part of the Andaman–Java subduction zone complex. The Indian plate subducts below the Burma–South East Asian plate along the Arakan–Yoma–Andaman–Java trench[5–7]. The Andaman and Nicobar Islands comprises of Cretaceous ophiolite and Tertiary sediments of outerarc-forearc in an accretionary prism setting[8]. In Rutland Island, dismembered bodies of Cretaceous ophiolite occur as thrust slices along with Tertiary sediments. The ophiolite consists of a tectonized ultramafic mantle sequence overlain by mafic–ultramafic crustal sequences. The different members of the Ophiolite group are exposed as: (1) lherzolite and diopsidic harzburgite of mantle sequence (2) cumulate sequence of ultramafic and mafic rocks, (3) intrusives of diorite–plagiogranite–boninite, and (4) volcanics of massive boninite and pillowed basalt interlayered with deep-sea pelagic sediments.

Mantle rocks of lherzolite to diopsidic harzburgite composition of Rutland ophiolite are partially serpentinized containing olivine, orthopyroxene, clinopyroxene and Cr-spinels as primary phases. In general, the mantle rocks show porphyroclastic textures[9]. Grain boundaries of large orthopyroxene and clinopyroxene porphyroclasts are irregular and strongly lobate. Deformed clinopyroxene porphyroclasts are locally surrounded by small neoblastic olivine grains (Figure 1 *a*). Pyroxene grains are partly replaced by olivine grains along cleavage planes and grain periphery. These textures develop due to melt–rock interaction involving dissolution of pyroxenes and crystallization of olivine when the olivine saturated basaltic melts ingress into mantle harzburgite specially in the subduction zone[10,11].

Orthopyroxene grains show three modes of occurrence: (i) large grains exhibiting exsolution of clinopyroxene, Cr-spinel and *n*-spinel (Opx-1), (ii) symplectites with Cr-spinel (Opx-2) and (iii) few homogenous grains (Opx-3). Clinopyroxene, other than exsolved lamellae (Cpx-1),

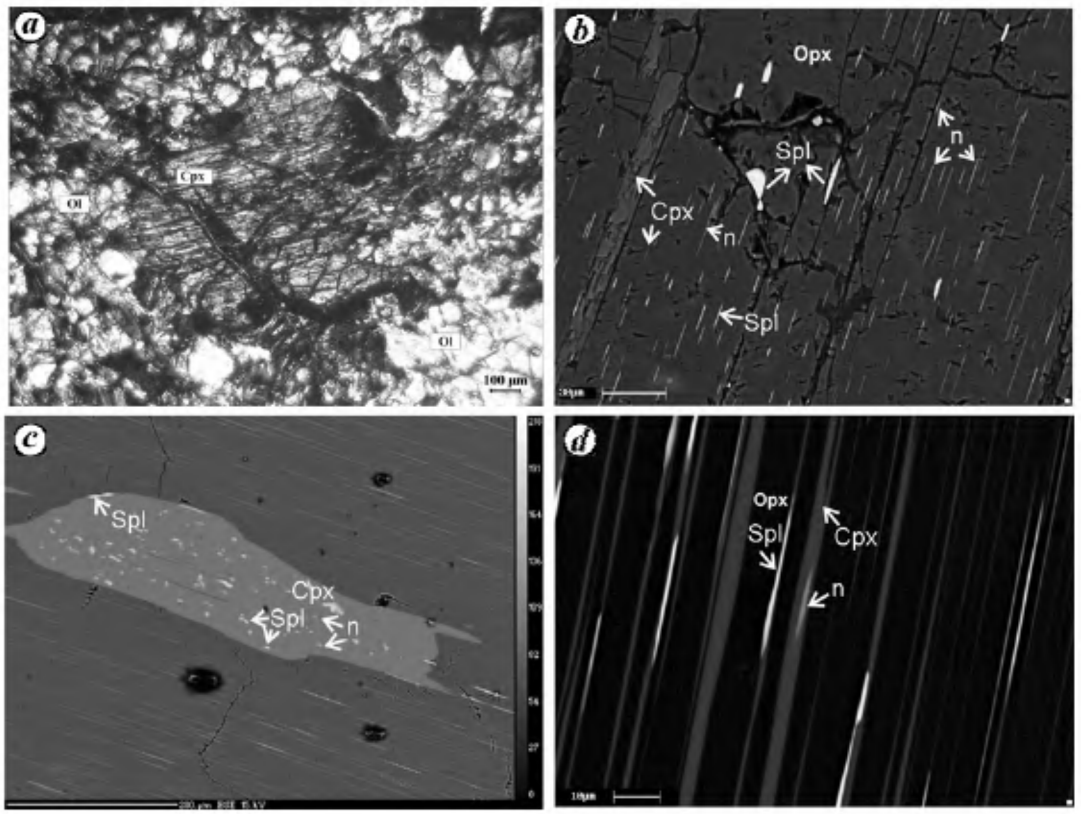

Figure 1. ***a***, Photomicrographs of clinopyroxene porphyroclasts with embayed margin surrounded by small olivine grains (under crossed nicols) (ol: olivine, cpx: clinopyroxene); ***b***, Back scattered image of fine exsolution lamellae of clinopyroxene, new phase (*n*-spinel) and Cr-spinel oriented in same direction within orthopyroxene host (opx: orthopyroxene, cpx: clinopyroxene, n: new phase, sp: Cr-spinel); ***c***, Back scattered image showing development of very small blebs of new phase and Cr-spinel within thick blebs of clinopyroxene. New phase occurs as very fine lamellae within host orthopyroxene (annotation same as Figure 1 *b*); ***d***, Back scattered image showing the distinct tonal difference of Cr-spinel (bright white) and new phase (greyish white) occurring as lamellae within orthopyroxene host (annotation same as Figure 1 *b*).

also occurs as unexsolved grain (Cpx-2). The Opx-1 grains contain thin to thick lamellae of Cpx-1 in the form of blebs and thin lamellae of Cr-spinel and *n*-spinel where the lamellae of *n*-spinel show thickness ranging from less than a micron to a maximum of 7 μ (Figure 1 *b*). Sometimes, the Cpx-1 occurring as blebs also contain very fine blebs of Cr-spinel and *n*-spinel (Figure 1 *c*), which are mostly aligned in long dimension. The lamellae of *n*-spinel are always intimately associated with Cpx-1 and Cr-spinel lamellae and show tonal character intermediate of Cr-spinel and diopside (Cpx-1; Figure 1 *d*). The representative samples of mantle harzburgite show modal composition as: 50–55 vol% olivine, 23–25 vol% orthopyroxene, 15–20 vol% clinopyroxene and 5–10 vol% Cr-spinel. These modal percentages were used for computation in bulk composition in PERPLEX program (described later). The modal analyses of Opx-1 grains show abundances of Cpx-1 (14–15 vol%) over Cr-spinel (3–6 vol%) and *n*-spinel (0.2–1.0 vol%) within the orthopyroxene host. Intergrown pyroxene and vermicular Cr-spinel at places show symplectitic growth. Interestingly, the symplectitic grains do not show any association with *n*-spinel.

Mineral chemistry from thin polished slides was obtained by CAMECA SX-100, housed at Central Petrological Laboratory, Geological Survey of India, Kolkata using wavelength dispersive spectrometry (WDS) at an acceleration voltage of 15 kV and a beam current of 12 nA and beam diameter of 1 μm. Instrument calibration was performed using natural mineral standards supplied by BRGM, France and results were corrected with a PAP matrix correction program. The standards were analysed at regular intervals to check the precision of sample analysis and 4–8 analytical points were used to calculate the average composition.

The composition of *n*-spinel with SiO_2: 14.06–22.08 wt%, Al_2O_3: 21.12–27.90 wt%, MgO: 15.67–18.53 wt%, FeO: 10.33–15.92 wt%, Cr_2O_3: 16.80–20.61 wt% and CaO: 4.38–9.7 wt% (Table 1) suggests that it could be designated as high-Si, high-Ca spinel-like phase. The analyses give a first hand impression that these could be mixed analyses of clinopyroxene and chromite. But the analyses of grains with different orientations yielding similar result suggest that the analyses are representative of discrete phases.

The orthopyroxene grains (Opx-1) hosting lamellae of Cpx-1, *n*-spinel and Cr-spinel show bronzitic to enstatitic composition (En_{88-92}). The symplectitic orthopyroxenes (Opx-2) as well as the homogenous grains (Opx-3) are also bronzitic (En_{88-90}). The Cpx-1 lamellae are diopside ($En_{46-49}Wo_{48-51}$; Table 2). On the other hand, the homogeneous clinopyroxene grains (Cpx-2) occur mostly as pigeonite which show a gradual increase in MgO and corresponding decrease in CaO contents from core ($En_{81}Wo_{11}$) to rim ($En_{89}Wo_1$). The unexsolved clinopyroxene grains occurring in association with symplectite orthopyroxene, however, show augite ($En_{67}Wo_{28}$) composition. The neoblastic olivine grains associated with both the homogenous and exsolved pyroxene grains are forsteritic (Fo_{89-91}) with no chemical zoning from core to rim (Table 3). The Cr-spinel shows a wide chemical variation with Mg#: 52–58, Cr#: 34–53, Fe#: 6–8 for homogenous grains; Mg#: 49–54, Cr#: 37–57, Fe#: 5–8 for exsolved lamellae and Mg#: 43–63, Cr#: 44–62, Fe#: 6–10 for symplectitic grains (Table 4).

The temperatures were determined using PTMAFIC programme with three thermometers, viz. olivine–spinel–orthopyroxene, orthopyroxene–clinopyroxene and olivine–spinel assemblages. The olivine–Cr-spinel–Opx-3 assemblage marked by 1, 2 in Tables 2–4 records near crystallization temperature as 960–1000°C (ref. 12). Using the same thermometer, the olivine–Cr-spinel–Opx-1 assemblage marked by 3 in Tables 2–4 yields a low temperature of 530°C and Opx-1–Cpx-1 assemblage marked by 4 in Table 2 yields 570°C (ref. 13). On the other hand, the olivine–Opx-2–Cr-spinel assemblage marked by 5 in Tables 2–4 records 860°C (ref. 12). The olivine–spinel assemblage marked by 6 in Tables 2 and 3 records re-equilibration temperature as 700°C (ref. 14). The mantle rocks, therefore, records four thermal events.

A probable range for the P–T conditions for the subsolidus relations could be observed from the pseudosection constructed for a representative bulk composition using the computer program PERPLEX (ref. 15; Figure 2). The activities of the minerals based on models of Holland and Powell[16] are included in the PERPLEX program. In that program, Cr_2O_3 could not be included in the activity of spinel. If that model had a scope to include Cr_2O_3, then spinel field could have been extended marginally towards the lower pressure boundary. The stability fields of the observed assemblages of olivine, spinel and pyroxene assemblages, therefore, in absence of

Table 1. Electron probe microanalysis of new phase from Rutland Island

Sample no.	10	10	10	10	88F
Rock	Lherzolite	Lherzolite	Lherzolite	Lherzolite	Diopsidic harzburgite
SiO_2	14.06	16.65	21.08	22.08	20.54
Al_2O_3	27.90	27.82	26.47	23.33	21.12
MgO	15.67	16.22	18.34	15.85	18.53
Na_2O	0.02	0.00	0.10	0.04	0.03
K_2O	0.00	0.00	0.00	0.00	0.04
CaO	7.33	8.05	4.38	9.70	4.05
TiO_2	0.00	0.05	0.00	0.02	0.00
FeO	13.03	12.61	13.15	10.33	15.92
MnO	0.05	0.13	0.11	0.08	0.26
Cr_2O_3	20.61	19.79	16.80	19.33	17.46
NiO	nd	nd	0.11	nd	0.17
Total	98.67	101.33	100.54	100.77	98.12

nd, Not determined.

Table 2. Electron probe microanalysis of pyroxene of mantle peridotite of Rutland Island

Sample	96	96	10	10	10	10	10	10	10	10	10	88f	88f	88f
Mineral	Opx	Opx	Cpx	Cpx	Cpx	Opx	Cpx	Cpx	Cpx	Opx	Cpx	Cpx	Cpx	Opx
Rock type	Diopsidic harzburgite	Diopsidic harzburgite	Lherzolite	Lherzolite	Lherzolite	Lherzolite	Lherzolite	Lherzolite	Lherzolite	Lherzolite	Lherzolite	Diopsidic harzburgite	Diopsidic harzburgite	Diopsidic harzburgite
Nature of grain	a (core)	a (rim)	a (core)	a (rim)	b (lamellae)	b (host)	b (lamellae)	b (lamellae)	b (lamellae)	c	c	c	c	b (host)
Thermometric pair	1	2			4	4				5				3
SiO_2	57.72	58.21	53.35	53.80	53.47	56.49	53.75	53.51	52.51	55.94	53.95	52.21	52.10	55.46
TiO_2	0.00	0.00	0.07	0.01	0.06	0.00	0.03	0.00	0.00	0.00	0.04	0.04	0.03	0.04
Al_2O_3	1.59	1.61	3.34	2.62	1.51	2.12	1.75	1.43	1.17	1.36	1.60	5.21	5.06	1.95
FeO	6.30	6.09	5.55	5.96	1.79	6.03	1.71	1.93	1.87	6.32	1.79	2.45	2.77	6.10
MnO	0.13	0.10	0.14	0.11	0.09	0.11	0.06	0.04	0.13	0.13	0.00	0.10	0.01	0.07
MgO	32.37	32.51	29.33	33.74	16.96	33.74	17.43	16.82	17.78	30.51	16.96	21.28	21.60	34.33
CaO	0.53	0.35	5.31	1.62	25.09	0.87	24.91	25.58	24.56	0.49	25.33	12.38	12.87	0.73
Na_2O	0.00	0.00	0.03	0.00	0.06	0.02	0.07	0.05	0.07	0.05	0.08	0.88	0.89	0.00
K_2O	0.00	0.00	0.01	0.00	0.00	0.00	0.00	0.00	0.00	0.00	0.00	0.00	0.00	0.04
Cr_2O_3	0.27	0.31	1.93	1.05	0.38	0.46	0.42	0.38	0.28	0.33	0.44	1.37	0.81	0.72
NiO	0.00	0.19	0.00	0.13	0.07	0.01	0.04	0.09	0.02	0.00	0.00	0.00	0.01	0.14
Total	98.91	99.37	99.06	99.04	99.48	99.85	100.17	99.83	98.39	95.13	100.19	95.92	96.15	99.58
TSi	2.025	2.033	1.887	1.872	1.953	1.952	1.946	1.949	1.931	2.047	1.957	1.929	1.916	1.918
TAl	0.000	0.000	0.113	0.107	0.047	0.048	0.054	0.051	0.051	0.000	0.043	0.071	0.084	0.079
TFe_3	0.000	0.000	0.000	0.020	0.000	0.000	0.000	0.000	0.000	0.000	0.000	0.000	0.000	0.002
M_1Al	0.066	0.066	0.026	0.000	0.018	0.038	0.021	0.011	0.000	0.059	0.025	0.155	0.135	0.000
M_1Ti	0.000	0.000	0.002	0.000	0.002	0.000	0.001	0.000	0.000	0.000	0.001	0.001	0.001	0.001
M_1Fe_3	0.000	0.000	0.032	0.098	0.018	0.000	0.025	0.032	0.000	0.000	0.009	0.000	0.000	0.061
M_1Fe_2	0.000	0.000	0.000	0.000	0.025	0.000	0.000	0.027	0.016	0.000	0.035	0.000	0.000	0.000
M_1Cr	0.007	0.009	0.054	0.029	0.011	0.013	0.012	0.011	0.008	0.010	0.013	0.040	0.024	0.020
M_1Mg	0.927	0.920	0.887	0.869	0.924	0.949	0.941	0.914	0.975	0.932	0.917	0.804	0.840	0.914
M_1Ni	0.000	0.005	0.000	0.004	0.002	0.000	0.001	0.003	0.001	0.000	0.000	0.000	0.000	0.004
M_2Mg	0.766	0.773	0.660	0.881	0.000	0.789	0.000	0.000	0.000	0.733	0.000	0.368	0.344	0.856
M_2Fe_2	0.185	0.178	0.132	0.055	0.011	0.174	0.027	0.000	0.041	0.193	0.010	0.076	0.085	0.113
M_2Mn	0.004	0.003	0.004	0.003	0.003	0.003	0.002	0.001	0.004	0.004	0.000	0.003	0.000	0.002
M_2Ca	0.020	0.013	0.201	0.060	0.982	0.032	0.966	0.998	0.968	0.019	0.984	0.490	0.507	0.027
M_2Na	0.000	0.000	0.002	0.000	0.004	0.001	0.005	0.004	0.005	0.004	0.006	0.063	0.063	0.000
M_2K	0.000	0.000	0.000	0.000	0.000	0.000	0.000	0.000	0.000	0.000	0.000	0.000	0.000	0.002
WO	1.0	0.7	10.5	3.0	50.0	1.7	49.3	50.6	48.3	1.0	50.3	28.1	28.5	1.4
EN	89.0	89.7	80.7	88.1	47.0	89.2	48.0	46.3	48.6	88.5	46.9	67.3	66.6	89.6
FS	9.9	9.6	8.8	8.9	2.9	9.1	2.7	3.0	3.1	10.5	2.8	4.5	4.8	9.0

a, Homogeneous grain; b, Exsolved grain; c, Symplectitic grain; Opx, Orthopyroxene; Cpx, Clinopyroxene.

Table 3. Electron probe microanalysis of olivine of mantle peridotite of Rutland Island

Sample	96	96	96	96	96	96	96	96	10	10	88F	88F	88F
Rock type	Diopsidic harzburgite	Diopsidic harzburgite	Diopsidic harzburgite	Diopsidic harzburgite	Diopsidic harzburgite	Diopsidic harzburgite	Diopsidic harzburgite	Diopsidic harzburgite	Lherzolite	Lherzolite	Diopsidic harzburgite	Diopsidic harzburgite	Diopsidic harzburgite
Nature of grain	a (core)	a (rim)	a (core)	a (rim)	a (rim)	a (core)	a (rim)	a (rim)	b (core)	b (rim)	b (core)	b (core)	b (rim)
Thermometric pair	1	2							5, 6		3		
SiO_2	41.27	40.99	41.46	41.19	40.88	41.15	41.14	41.35	40.89	40.53	40.67	40.39	40.56
TiO_2	0.00	0.00	0.00	0.00	0.00	0.00	0.02	0.00	0.00	0.00	0.02	0.00	0.00
Al_2O_3	0.00	0.00	0.02	0.00	0.03	0.01	0.00	0.00	0.00	0.00	0.00	0.00	0.00
FeO	9.17	9.23	8.97	8.74	9.23	8.79	8.96	8.90	8.30	9.07	8.94	8.91	11.08
MnO	0.14	0.06	0.17	0.17	0.04	0.10	0.06	0.15	0.12	0.18	0.17	0.13	0.14
MgO	47.80	47.11	46.63	46.77	47.89	46.90	47.45	47.41	48.52	47.73	49.86	49.33	48.23
CaO	0.00	0.00	0.01	0.00	0.00	0.00	0.00	0.00	0.01	0.00	0.01	0.00	0.08
Na_2O	0.07	0.00	0.00	0.00	0.02	0.00	0.00	0.01	0.04	0.02	0.04	0.04	0.02
K_2O	0.02	0.02	0.01	0.02	0.00	0.00	0.01	0.01	0.00	0.00	0.00	0.00	0.02
NiO	0.65	0.36	0.39	0.50	0.49	0.44	0.47	0.61	0.31	0.57	0.21	0.51	0.28
Total	99.12	97.77	97.66	97.39	98.58	97.39	98.11	98.44	98.19	98.10	99.92	99.31	100.41
Si	1.018	1.023	1.034	1.030	1.013	1.029	1.022	1.024	1.013	1.011	0.995	0.995	0.997
Al	0.000	0.000	0.001	0.000	0.001	0.000	0.000	0.000	0.000	0.000	0.000	0.000	0.000
Ti	0.000	0.000	0.000	0.000	0.000	0.000	0.000	0.000	0.000	0.000	0.000	0.000	0.000
Fe_2	0.189	0.193	0.187	0.183	0.191	0.184	0.186	0.184	0.172	0.189	0.183	0.184	0.228
Mn	0.003	0.001	0.004	0.004	0.001	0.002	0.001	0.003	0.003	0.004	0.004	0.003	0.003
Mg	1.757	1.753	1.733	1.743	1.770	1.748	1.758	1.751	1.792	1.774	1.818	1.812	1.767
Ca	0.000	0.000	0.000	0.000	0.000	0.000	0.000	0.000	0.000	0.000	0.000	0.000	0.002
Na	0.003	0.000	0.000	0.000	0.001	0.000	0.000	0.000	0.002	0.001	0.002	0.002	0.001
K	0.001	0.001	0.000	0.001	0.000	0.000	0.000	0.000	0.000	0.000	0.000	0.000	0.001
Ni	0.013	0.007	0.008	0.010	0.010	0.009	0.009	0.012	0.006	0.011	0.004	0.010	0.006
Fo	90.3	90.1	90.3	90.5	90.3	90.5	90.4	90.5	91.2	90.4	90.9	90.8	88.6
Fa	9.7	9.9	9.7	9.5	9.7	9.5	9.6	9.5	8.8	9.6	9.1	9.2	11.4

a, Associated with homogeneous pyroxene grain; b, Associated with exsolved pyroxene grain.

Table 4. Electron probe microanalysis of Cr-spinel of mantle peridotite of Rutland Island

Sample	96	96	10	10	10	10	10	88f	88f	88f
Rock type	Diopsidic harzburgite	Diopsidic harzburgite	Lherzolite	Lherzolite	Lherzolite	Lherzolite	Lherzolite	Diopsidic harzburgite	Diopsidic harzburgite	Diopsidic harzburgite
Nature of grain	a	a	a	b	c	c	c	c	c	b
Thermometric pair	1, 2				5, 6					3
SiO_2	0.05	0.01	0.00	0.00	0.00	1.64	0.00	0.03	0.01	0.23
TiO_2	0.00	0.01	0.05	0.03	0.09	0.04	0.01	0.00	0.00	0.00
Al_2O_3	34.93	23.57	23.29	33.58	23.18	26.71	22.52	18.13	17.73	20.70
FeO	24.33	29.46	22.49	22.40	23.25	21.89	23.94	27.02	27.30	25.23
MnO	0.12	0.48	0.15	0.19	0.24	0.20	0.19	0.40	0.18	0.32
MgO	11.55	8.84	12.61	12.18	11.83	13.97	10.07	8.95	8.82	10.17
CaO	0.00	0.02	0.00	0.01	0.00	0.00	0.01	0.11	0.07	0.14
Na_2O	0.03	0.04	0.03	0.03	0.00	0.04	0.00	0.01	0.10	0.02
K_2O	0.00	0.01	0.00	0.00	0.00	0.01	0.01	0.00	0.08	0.01
Cr_2O_3	26.35	34.42	39.98	29.76	41.33	34.15	40.85	42.80	42.46	40.55
NiO	0.11	0.17	0.13	0.22	0.10	0.10	0.06	0.00	0.20	0.00
Total	97.61	97.03	98.73	98.55	100.03	98.75	97.95	97.58	97.02	97.51

a, Homogenous grain; b, Exsolved grain; c, Symplectitic grain.

plagioclase and garnet in the present study, could not be changed much even after Cr_2O_3 was entered into the computation. In that case, we can presume that the pseudosection so constructed holds good for the present assemblages. An independent temperature estimate as done in the present case using PTMAFIC program can, therefore, reasonably bracket the pressure range over which a given assemblage could be stable for a specific bulk composition.

The assemblage of olivine-homogenous orthopyroxene–spinel recorded equilibrium temperature at 960–1000°C (ref. 17). At that temperature, pressure is approximated in the pseudosection as 10 kb (Figure 2). The pyroxene–Cr-spinel symplectites recording 860°C bracket the pressure range from 8 to 10 kb (Figure 2). The bulk re-equilibration involving Fe–Mg exchange in olivine–spinel is controlled dominantly by temperature. At 700°C temperature, the process yields similar pressure range (8–10 kb). The exsolution of clinopyroxene within host orthopyroxene, being a cooling dominated event, occurred at the same pressure range, i.e. 8–10 kb.

Exsolution of pyroxene–spinel and orthopyroxene–clinopyroxene has been reported from many mantle xenoliths and peridotite of ophiolite sequence[2,18–20]. The exsolution of spinel and diopside from aluminous enstatite or pigeonite could be due to solid solution of non-stoichiometric pyroxene and spinel[9]. The exsolved Cr-spinel, clinopyroxene and *n*-spinel are, therefore, derived solely from the pre-existing pyroxene. On an average, exsolved Cr-spinel with 26 wt% Al_2O_3 represents 5 vol% (inclusive of *n*-spinel), exsolved diopside with 1.5 wt% Al_2O_3 represents 15 vol% and the remaining 80 vol% orthopyroxene host contains 2 wt% Al_2O_3. The source for the alumina content of Cr-spinel and the *n*-spinel, therefore, could be either aluminous orthopyroxene or pigeonite. But considering the CaO contents in clinopyroxene and *n*-spinel, pigeonite source is preferred to aluminous orthopyroxene.

The assemblage of olivine–homogenous orthopyroxene–spinel recorded equilibrium temperature at 960–1000°C (ref. 17). At that temperature, the pseudosection pressure is around 10 kb. During upwelling of the mantle rocks, the pyroxene–Cr-spinel–symplectites developed at 860°C by the reaction of olivine and garnet during garnet–spinel transition. The bulk re-equilibration at 700°C reflected by olivine and spinel assemblage records subsolidus reaction in these mantle rocks. The exsolution of clinopyroxene–Cr-spinel–*n*-spinel took place with further drop of temperature at 530–570°C. The exsolution of clinopyroxene within host orthopyroxene, a cooling dominated event[21], occurred either during uprise or re-equilibration at shallower depths.

Experimental studies show that mixed Al_2O_3–SiO_2 gels during heating could be converted to spinel-type phase in the temperature range of 900–1000°C and could remain stable up to 1250°C (ref. 2). Incorporation of SiO_2 into alumina phase could start during heating above 1000°C. Such a process could occur at lower temperatures in high pH_2O condition. In the present case of subduction zone environment, prevalent high pH_2O condition possibly contributed to the entry of Si in spinel structure. The replacement of Al^{3+} by Si^{4+} led to distortion and charge imbalance of the crystallographic sites in spinel structure which was subsequently balanced by the entry of Ca^{2+}.

Symplectitic orthopyroxene–spinel could be derived during subsolidus reaction of olivine with garnet during garnet to spinel transitions[2].

In the spinel stability field, the exsolution process initiated due to cooling. During exsolution event at the first stage, blebs of pigeonite exsolved and subsequently high-

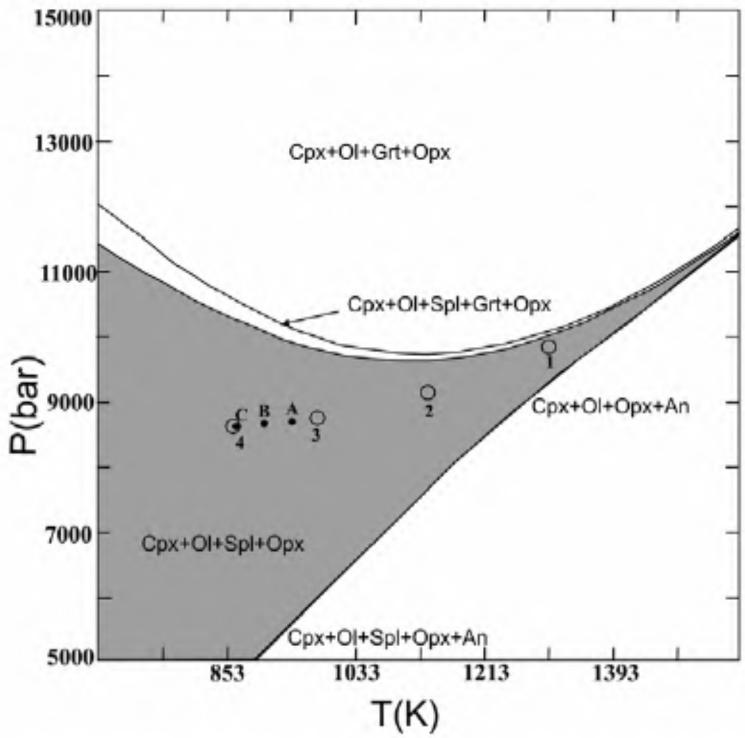

Figure 2. Numerically computed phase diagram (pseudosection) for a representative bulk composition of mantle rock. The stability field of the observed assemblages of olivine–pyroxene–spinel is shown by the area filled with grey colour. The hollow circles with numbers show the positions of different stages of the subsolidus reactions in the PT field. Stage 1: The upwelling of mantle rocks changing the domain of garnet field to spinel field producing the assemblage to olivine–homogenous orthopyroxene–spinel. Stage 2: The formation of pyroxene–spinel symplectite. Stage 3: The bulk re-equilibration involving Fe–Mg exchange in between olivine–spinel. Stage 4: Development of exsolution of clinopyroxene and spinel within orthopyroxene grain. The different substages for the change from stages 3 to 4 are also indicated by filled circles with capital letters in the diagram. Substage A: Clinopyroxene exsolved as thick blebs from the pre-existing pigeonite. Substage B: Fine blebs and lamellae of new phase (*n*-spinel) exsolved within clinopyroxene and orthopyroxene host. Substage C: Fine lamellae of *n*-spinel, Cr-spinel and clinopyroxene exsolved within host orthopyroxene.

Si, high-Ca bearing spinel-like intermediate phase (*n*-spinel) started to form. Afterwards, the fine lamellae of Cr-spinel and diopside exsolved from the pre-existing pigeonite. Petrographic features show that thick blebs of clinopyroxene exsolved in orthopyroxene contain minute blebs of *n*-spinel and spinel. Very fine exsolution lamellae of clinopyroxene, spinel and *n*-spinel also occur within the orthopyroxene host. These features suggest three steps of exsolution (Figure 2). At the first step, clinopyroxene exsolved as thick blebs from the pre-existing pigeonite consuming a high amount of CaO. During the second step, fine blebs and lamellae of new spinel-like phase (*n*-spinel) started to exsolve within the clinopyroxene and orthopyroxene hosts. In the third step, with further lowering of temperature fine lamellae of *n*-spinel, Cr-spinel and clinopyroxene exsolved within host orthopyroxene.

In the subduction regime of Andaman Islands, ophiolites occur as thrust slices in accretionary prism. Mantle rocks are emplaced to the surface by thrust forces. At the initial stage of uprise, garnet to spinel transition took place in the mantle rocks. During further uprise of the mantle rocks due to cooling, exsolution in pyroxene was the prevalent process in the spinel stability field. High pressure–temperature conditions coupled with melt contaminations possibly stabilized the high-Si, high-Ca spinel-like new phase in lherzolitic to diopsidic harzburgitic mantle peridotites. The new phase possibly formed in complex geochemical situations especially in subduction zone setting where mantle metasomatism was a predominant process. The stability field of such a phase is to be specified experimentally. Characterization of new spinel-like phase by XRD and other mineral parameters were limited due to their occurrence as fine lamellae or minute blebs. The new spinel-like phase occurred as an intermediate phase in spinel–pyroxene exsolution regime. The stability field as well as characterization of such a naturally occurring phase needs to be established by experiments. In light of the present study, the stability field of spinel in existing geotherms is to be modified for garnet–spinel transition.

1. Chakraborty, A. K., Range of solid solutions of silica in spinel type phase. *Adv. Appl. Ceram.*, 2006, **105**, 297–303.
2. Falus, G., Szabo, C., Kovacs, I., Zajacz, Z. and Halter, W., Symplectite in spinel lherzolite xenoliths from the Little Hungaria

Plain, Western Hungary: a key for understanding the complex history of the upper mantle of the Pannonian Basin. *Lithos*, 2007, **94**, 230–247.
3. Medaris, L. G., Fournelle, J. H., Wang, H. F. and Jelinek, E., Thermobarometry and reconstructed chemical compositions of spinel–pyroxene symplectites: evidence for pre-existing garnet in lherzolite xenolith from Czech Neogene lavas. *Russ. Geol. Geophys.*, 1997, **38**, 277–286.
4. Morishita, T. and Arai, S., Evolution of spinel–pyroxene symplectite in spinel lherzolites from the Horoman Complex, Japan. *Contrib. Mineral. Petrol.*, 2003, **144**, 509–522.
5. Curray, J. R. and Moore, D. G., Sedimentary and tectonic processes in the Bengal deep sea fan and geosyncline. In *The Geology of Continental Margins* (eds Burke, C. A. and Drake, C. L.), Springer, New York, 1974.
6. Karig, D. E., Suparka, S., Moore, G. F. and Hehanussa, P. E., Structure and Cenozoic evolution of the Sunda arc in the Central Sumatra Region. In *Geological and Geophysical Investigations of Continental Margin* (eds Watkins, J. S., Montadert, L. and Dickinson, P. W.), Mem. Am. Assoc. Petrol. Geol., 1979, p. 29.
7. Mukhopadhyay, M., Gravity anomalies and deep structure of the Andaman Arc. *Mar. Geophys. Res.*, 1988, **9**, 197–211.
8. Pal, T., Chakraborty, P. P., Duttagupta, T. and Singh, C. D., Geodynamic evolution of an outer arc in convergent margin of active Burma–Java subduction complex, a document from Andaman islands, Bay of Bengal. *Geol. Mag.*, 2003, **140**, 289–307.
9. Mercier, J. C. C. and Nicolas, A., Textures and fabrics of upper mantle peridotites as illustrated by xenoliths from basalts. *J. Petrol.*, 1975, **6**, 454–487.
10. Dick, H. J. B., Abyssal peridotites, very slow spreading ridges and ocean ridge magmatism. In *Magmatism in the Ocean Basins* (eds Saunders, A. D. and Norry, M. J.), Geol. Soc. London, Spec. Publ., 1989, vol. 42, pp. 71–105.
11. Kelemen, P. B., Joyce, D. M., Webster, J. D. and Holloway, J. R., Reaction between ultramafic rock and fractionating basaltic magma, II, Experimental investigation of reaction between olivine tholeiite and harzburgite at 1050–1150°C and 5 kbar. *J. Petrol.*, 1990, **31**, 99–134.
12. Gasparik, T. and Newton, R. C., The reversed alumina contents of orthopyroxene in equilibrium with spinel and forsterite in the system $MgO–Al_2O_3–SiO_2$. *Contrib. Mineral. Petrol.*, 1984, **85**, 186–196.
13. Wood, B. J. and Banno, S., Garnet–orthopyroxene and orthopyroxene–clinopyroxene relationships in simple and complex systems. *Contrib. Mineral. Petrol.*, 1973, **42**, 109–124.
14. Ballhaus, C., Berry, R. F. and Green, D. H., High-pressure experimental calibration of the olivine–orthopyroxene–spinel oxygen barometer: implications for the oxidation state of the mantle. *Contrib. Mineral. Petrol.*, 1991, **107**, 27–40.
15. Connolly, J. A. D., Computation of phase equilibria by linear programming: a tool for geodynamic modelling and its application to subduction zone decarbonation. *Earth Planet. Sci. Lett.*, 2005, **236**, 524–541.
16. Holland, T. J. B. H., and Powell, R., An internally consistent thermodynamic data set for phases of petrological interest. *J. Metamorph. Geol.*, 1998, **16**, 309–343.
17. O'Neill, H. StC., The transition between spinel lherzolite and its use as a geobarometer. *Contrib. Mineral. Petrol.*, 1981, **77**, 185–194.
18. Smith, D., The origin and interpretation of spinel–pyroxene clusters in peridotite. *J. Geol.*, 1976, **85**, 476–482.
19. Nicolas, A., Lucazeau, F. and Bayer, R., Peridotite xenolith in Massif Central basalts, France: textural and geophysical evidence for asthenospheric diapirism. In *Mantle Xenoliths* (ed. Nixon, P. H.), John Wiley and Sons, Chichester, 1987.
20. Luhr, F. and Aranda Gomez, J. J., Mexican peridotite xenoliths and tectonic terranes: correlation among vent location, texture, temperature, pressure and oxygen fugacity. *J. Petrol.*, 1997, **38**, 1075–1112.
21. Brey, G. P. and Kohler, T. P., Geothermobarometry in four phase lherzolites, part II: new thermobarometers, and practical assessment of existing thermobarometers. *J. Petrol.*, 1990, **31**, 1353–1378.

ACKNOWLEDGEMENTS. We thank Dr A. Roy, Dy. Director General, GSI, Eastern Region, Dr S. Ghosh, Director, Petrology Division and Dr U. Chakraborty, Director, for support. We acknowledge the help of S. K. Shome, SEM Lab, Kolkata, Sri B. Chattopadhyay, Dr S. Sengupta, and Sri S. Nandy, EPMA Lab, Kolkata.

Received 23 October 2008; revised accepted 6 August 2009